PHYSICAL REVIEW B VOLUME 40, NUMBER 1 1 JULY 1989

Green's functions for antiferromagnetic polaritons. I. Surface modes and resonances

R. L. Stamps
Department of Physics, Colorado State University, Fort Collins, Colorado 80532

R. E. Camley
Department of Physics, University of Colorado, Colorado Springs, Colorado 80933
(Received 29 July 1988)

We calculate the classical electromagnetic Green's functions for antiferromagnetic polaritons on a semi-infinite geometry. With damping present in the material, surface resonances are found that exist in frequency and wavelength regions forbidden to surface-polariton modes. These resonances are identified as magnetic analogs of the evanescent and Brewster modes found in plasmon-polariton studies. These antiferromagnetic surface resonances have finite path lengths and large penetration depths into the material which are very sensitive to material damping and externally applied fields.

I. INTRODUCTION

The coupling between electromagnetic waves and the fundamental excitations in a material (plasmons, phonons, etc.) produces what is known as a polariton. Polaritons in dielectrics and metals have been extensively studied both theoretically and experimentally. Surface polaritons in dielectrics and metals, where the amplitude of the excitation is confined to the region near the surface, have also received a great deal of attention[1] and are now used as a tool in studying the vibrational spectra of very thin films.[2]

In contrast, magnetic polaritons,[3] coupled electromagnetic waves and spin waves, and magnetic surface polaritons[4] have received less attention. One reason for this is that in ferromagnets the frequency of the magnetic polariton is typically lower (1–20 GHz for metallic ferromagnets) than the frequency for a phonon-polariton. This means wavelengths for ferromagnetic polaritons are generally much larger than for phonon-polaritons and it is difficult to realistically obtain an effectively infinite or semi-infinite sample size or to obtain information about the region close to the surface.

Recently the properties of bulk and surface polaritons on a semi-infinite uniaxial *antiferromagnet* were discussed theoretically and measured by Remer *et al.* on MnF_2 using reflectivity measurements.[5] These excitations possess several intriguing features. First, and in contrast to the ferromagnet, antiferromagnetic polaritons have frequencies in the infrared with typical values ranging from 250 GHz to a few THz. The wavelengths (and penetration depths) thus range from millimeters to a few hundred micrometers. Second, and in contrast to phonon-polaritons, antiferromagnetic surface polaritons are nonreciprocal,[6] i.e., $\omega(+k)\neq\omega(-k)$. For nonreciprocal surface waves, reversing the direction of propagation or reversing the direction of an applied magnetic field generally leads to a surface polariton of a different frequency. The degree of nonreciprocity can be controlled by varying the strength of the applied field and disappears when the applied field is turned off.

To date, theoretical discussions of the properties of antiferromagnetic polaritons have focused on dispersion relations calculated from the electromagnetic wave equation for anisotropic magnetic media.[7] Dispersion curves describe the possible allowed modes of the magnetic system, but do not describe how these modes may be excited. It is often useful, however, to know the response of the magnetic system to some external probe—such as the response of an antiferromagnet to an incident light wave. Green's functions are a primary tool for dealing with these types of questions.[8]

The main objective of this paper is to calculate the electromagnetic Green's functions for a semi-infinite antiferromagnet. As usual, Green's functions can be used to obtain a variety of information about the allowed modes of a system. Dispersion relations, spectral densities, and the effective lifetime or attenuation length can all be obtained from the Green's functions.[9] In addition, Green's functions can be used in a variety of applications. Examples include the calculation of Raman and Brillouin scattering spectra, nonlinear interactions of surface polaritons, and thermodynamic properties.[10–12] In the following paper (hereafter referred to as paper II) we will use these Green's functions to study the reflectivity from an antiferromagnet with a slightly rough surface.

Our second major goal is to discuss the effects of damping on polariton modes in antiferromagnets. There are several reasons for this. Damping often plays a critical role in the interaction of external probes with polaritons. For example, in the reflection experiment mentioned earlier, damping is necessary for a coupling of the external electromagnetic radiation to the surface polariton modes. As we will see in this paper, damping not only has a significant impact on the surface polariton modes discussed in earlier works, but the inclusion of damping also leads to the existence of new "leaky" surface modes.

The leaky surface modes we find in this magnetic system are analogous to the Brewster surface-polariton modes found in dielectric materials. As is well known, for a wave incident on a nonabsorbing dielectric and E field polarized in the plane of incidence, there exists an

angle of incidence for which there is no reflected wave. Since the Brewster angle depends on the frequency ω, it provides a relationship between ω and k_x, the component of the wave vector parallel to the surface. With damping included, one can find a solution of Maxwell's equations for a weakly bound surface wave which decays as it propagates parallel to the surface. This surface mode has a dispersion relation ω as a function of $\mathrm{Re}(k_x)$ which is very similar to the relationship in the Brewster case and is known as a Brewster mode.[13] In our antiferromagnetic system, we find a very equivalent result. Here a Brewster angle occurs for a geometry where the magnetic field lies in the plane of incidence. Again when damping is present, a magnetic Brewster surface mode can exist with a dispersion relation similar to that provided by the relationship of the magnetic Brewster's angle and the frequency.

The paper begins with a study of the effects of damping on the semi-infinite antiferromagnetic polariton curves and discusses the properties of the magnetic Brewster mode. Next we calculate the Green's functions appropriate to a semi-infinite antiferromagnet. Due to the complexity of the algebra, we restrict ourselves to incident and scattered fields which are polarized with electric fields parallel to the easy axis. Finally we study the magnetic Brewster mode through the behavior of the Green's functions and show a correspondence between the peaks of the Green's functions and the solutions to the damped dispersion relations for frequencies near the antiferromagnetic resonance frequencies.

II. SURFACE POLARITONS WITH DAMPING

A more realistic description of surface polaritons is obtained by including a damping mechanism in the equations of motion. In general, damping affects the degree of localization of the wave to the surface and causes the wave to lose energy as it propagates. Although damping and its effects on surface polaritons has been studied for plasmon polaritons and magnetoelastic polaritons on ferromagnets, antiferromagnetic surface polariton studies have only considered the idealized case of zero damping. In this section damping is included in the description, and the resulting effects on the surface polariton's dispersion curve, path length, and penetration depth are examined.

In addition to modifying the properties of the "true" antiferromagnetic surface polaritons, the inclusion of damping shows the existence of new surface resonances, or "leaky" surface modes. These are very different in character from the modes found without damping. The "true" surface modes and the leaky modes are investigated by numerically examining the surface-polariton dispersion relation for the material MnF_2.

The geometry is shown in Fig. 1. The material is in the $y>0$ half-space with the surface at $y=0$. The antiferromagnet is uniaxial and the magnetizations of the two sublattices lie along the $\pm z$ axis. The applied field also lies along z. The dielectric properties are determined by the diagonal, though anisotropic, dielectric tensor:

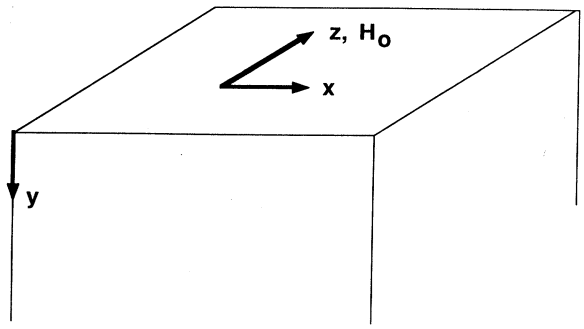

FIG. 1. Geometry for this paper. The material lies in the $y>0$ half space with the easy axis along z. An applied field is also set along the z axis. Propagation is in the $\pm x$ directions with the E field parallel to the z axis and H field in the xy plane.

$$\overleftrightarrow{\epsilon}=\begin{bmatrix}\epsilon_1 & 0 & 0\\ 0 & \epsilon_1 & 0\\ 0 & 0 & \epsilon_2\end{bmatrix}. \tag{2.1}$$

We will assume the dielectric susceptibilities are constant over the frequency ranges we are interested in for this paper, although it is a simple matter to substitute the appropriate frequency dependent functions for ϵ_1 and ϵ_2. The magnetic susceptibility tensor for a uniaxial antiferromagnet is

$$\overleftrightarrow{\mu}=\begin{bmatrix}\mu_1 & i\mu_2 & 0\\ -i\mu_2 & \mu_1 & 0\\ 0 & 0 & 1\end{bmatrix}. \tag{2.2}$$

The magnetic susceptibilities are frequency dependent and are found, for the long wavelength limit, by solving Bloch's equations of motion for the two sublattice system of spins.[14] The results can be written in the form

$$\mu_1=1-\frac{4\pi\gamma^2MH_a}{\Omega^2}(X+Y)\,, \tag{2.3}$$

$$\mu_2=\frac{4\pi\gamma^2MH_a}{\Omega^2}(Y-X)\,. \tag{2.4}$$

Here M is the magnitude of the sublattice magnetizations, H_a is the magnitude of the anisotropy field directing the spins along their respective sublattices, and Ω is the antiferromagnetic resonance field given by

$$\Omega^2=H_a\gamma^2(H_a+2H_e)\,, \tag{2.5}$$

where H_e is the exchange field. The quantities X and Y are defined as

$$X=[(\omega/\Omega+H_0\gamma/\Omega+i/\Omega\tau)^2-1]^{-1}\,, \tag{2.6}$$

$$Y=[(\omega/\Omega-H_0\gamma/\Omega+i/\Omega\tau)^2-1]^{-1}\,. \tag{2.7}$$

The applied field is H_0 and τ is a phenomenological spin relaxation time. γ is the gyromagnetic ratio. Outside the material, where $y<0$, the susceptibilities are uniform and

describe a vacuum:

$$\epsilon_{ij}=\delta_{ij} , \tag{2.8}$$

$$\mu_{ij}=\delta_{ij} . \tag{2.9}$$

The wave equation for propagation in media described by the susceptibilities (2.1) and (2.2) has the form

$$\epsilon_k \sum_{j,m}{}' \left[\epsilon_m^{-1} \frac{\partial^2}{\partial x_j \partial x_k} - \delta_{jk} \left[\sum_l \epsilon_m^{-1} \frac{\partial^2}{\partial x_l^2} \right] - \omega_0^2 \mu_{kj} \right] H_j = 0 . \tag{2.10}$$

The prime on the sum means that $m \neq j,k,l$. Here and throughout the rest of the paper, $\omega_0=\omega/c$. Since the dielectric tensor is diagonal in this problem, we set $\epsilon_{kk}=\epsilon_k$.

The dispersion relation for surface polaritons is obtained by assuming plane-wave solutions of the form

$$\exp[i(k_x x-\omega t)]\exp(-\alpha y)$$

inside the material and

$$\exp[i(k_x x-\omega t)]\exp(\beta y)$$

outside the material. The fields inside and outside the material are then matched according to Maxwell's boundary conditions on tangential H and normal B. The resulting implicit expression was derived by Camley and Mills:[7]

$$\beta+(\mu_1\alpha+\mu_2 k_x)/(\mu_1^2-\mu_2^2)=0 \tag{2.11}$$

k_x is the wave vector parallel to the surface, and decay in the y direction is governed by α and β. These are given by

$$\alpha=\left[k_x^2-\omega_0^2\epsilon_2 \left[\frac{\mu_1^2-\mu_2^2}{\mu_1^2} \right] \right]^{1/2} \tag{2.12}$$

and

$$\beta=(k_x^2-\omega_0^2)^{1/2} . \tag{2.13}$$

When there is no damping in the material, Eq. (2.12) can be satisfied by appropriate choices of real frequencies and real wave vectors. In this case both α and β are positive and real. These modes represent excitations that are bound to the surface, with infinite lifetimes. Also, when $H_0=0$ the modes are reciprocal in k. This means the solutions obey $\omega(k)=\omega(-k)$. In the presence of an applied field the modes are not reciprocal and the solutions obey $\omega(k)\neq\omega(-k)$.

Bulk modes, on the other hand, exist in frequency ranges where α is pure imaginary. One sees from (2.12) that these ranges exist for those ω, k_x such that $\alpha^2<0$. In an infinite geometry, all values of α are allowed and so the number of bulk modes is infinite in each bulk band. Also, the bulk modes are reciprocal in k_x both with and without an applied field.

When damping is present in the magnetic system [through τ in the susceptibilities of (2.3) and (2.4)], the dispersion Eq. (2.11) no longer possesses pure real wave-vector and frequency solutions. The dispersion relation can be satisfied, however, for real frequencies and complex wave vectors. With complex α, β, and k_x, these solutions represent dissipative waves that have finite path lengths.

To illustrate the properties of these dissipative waves, Eq. (2.11) was solved numerically for MnF_2 both with and without damping. The relevant parameters are $H_e=550$ kG, $H_a=7.87$ kG, $M=0.6$ kG, and $\epsilon_2=5.5$.[7] The quantities plotted below are unitless with reduced frequencies ω/Ω and reduced wave vector $k_x c/\Omega$ (the component parallel to the surface).

In Fig. 2 the dispersion relations for bulk and surface polaritons are reproduced for the case of $H_0=0$. The shaded areas represent the bulk modes and the dashed lines between the two bulk bands are surface modes for the case of zero damping. Note that these surface modes stop abruptly at the top of the lower bulk band where $k_x=\omega/c$. As the wavelength decreases, ω/k goes to zero and the surface polaritons asymptotically approach the zero-field magnetostatic surface wave[15] frequency given by

$$\omega_s=\gamma[H_a(2H_e+H_a+4\pi M)]^{1/2} .$$

In Fig. 2 the surface polariton solutions to (2.11) when $1/\omega\tau=0.0002$ are also included. These solutions are plotted as functions of reduced frequency and the real part of the reduced parallel wave vector. These dissipative waves lie very near the $1/\Omega\tau=0$ surface polaritons in

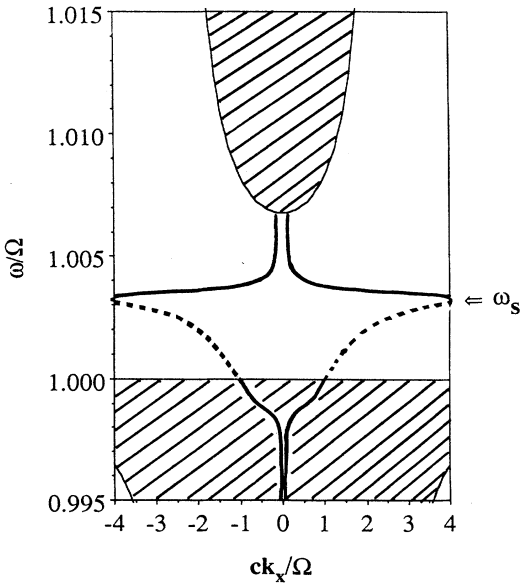

FIG. 2. Dispersion curves for antiferromagnetic polaritons, in MnF_2, with no applied field. The shaded areas are bulk bands and the dashed lines are the surface modes when there is no damping present. The solid lines show how damping modifies the surface mode frequencies. These solid lines are the real parts of the complex solutions to the dispersion relation (2.11), with damping $1/\Omega\tau=0.0002$.

the frequency region above the lower bulk band and below the magnetostatic frequency. Outside this region, new solutions appear and are represented by solid lines.

Above ω_s the dissipative waves exhibit a curious "backbending" property where the group velocity changes sign and the modes curve inward in k_x toward the upper bulk band. This backbending effect is reminiscent of a similar behavior found for surface plasmon-polaritons where the Fano ("true") surface modes bend back with increasing frequency into what are sometimes called evanescent modes.[13] The evanescent modes are tightly bound to the surface and the real and imaginary parts of the wave-vector component normal to the surface have roughly the same magnitude. It is interesting to note that since the point of backbending occurs near ω_s, the corresponding k_x can be used to measure the damping parameter. As the frequency increases above ω_s, the real parts of β and α become small so that the evanescent modes are less tightly bound to the surface. Near the lower limit of the upper bulk band, the real parts of β and α tend to zero and the evanescent modes become ill-defined.

With damping present, the polariton mode continues into the lower bulk band below the lower bulk band frequency limit, as seen in Fig. 2. This is a region forbidden to true surface polaritons. In this frequency region modes can exist, with damping present, at an ω and k_x for which a wave incident on the material from vacuum would be completely transmitted. We thus identify the $1/\Omega\tau=0.0002$ mode as the magnetic analogue of the Brewster mode found in dielectric materials.

Typically, one thinks of the Brewster angle as the angle of incidence where there is no reflected wave from a surface illuminated by a wave polarized with its electric field in the plane of incidence. A similar angle occurs for a wave incident on a magnetic material and polarized with its magnetic field in the plane of incidence. This angle (or rather the corresponding component of the incident wave vector, k_x) can be found by setting to zero the amplitude of the magnetic field of the reflected wave (see the appendix of the companion paper for the appropriate Fresnel relations). Doing so, one arrives at the magnetic Brewster condition:

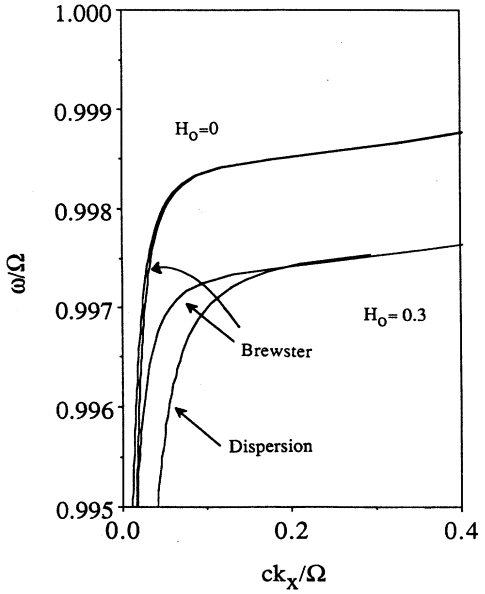

FIG. 3. Real part of the complex dispersion solutions compared to the Brewster angle (in terms of k_x rather than θ_0). The upper curves are for $H_0=0$ and the lower curves are for the $-k_x$ branch of the surface-polariton dispersion with $H_0=0.3$ kG. In the $H_0=0$ case, the curves are identical at higher frequencies.

$$(k_x)_{\mathrm{Br}}=\omega_0[\mu_1\epsilon_2(\mu_1^2-\mu_2^2)-(\mu_1^2-\mu_2^2)^2]/[\mu_1^2-(\mu_1^2-\mu_2^2)^2]^{1/2}\ . \tag{2.14}$$

In Fig. 3 the ω and k_x that satisfy Eq. (2.14) are plotted along with the solutions to the dispersion relation (2.11) for $1/\Omega\tau=0.0002$. The real part of the complex wave-vector solutions are plotted against the frequency both with an applied field and without. When there is no applied field there is a very close correspondence between the two curves. When $H_0=0.3$ kG, however, the two curves begin to differ for frequencies well within the lower bulk band.

Since $\mathrm{Re}(\alpha)$ determines how tightly the surface wave is bound to the surface and $\mathrm{Im}(k_x)$ governs the attenuation of the wave as it propagates parallel to the surface, it is interesting to plot these quantities as functions of frequency. In Fig. 4, $|\mathrm{Im}(ck_x/\Omega)|$ is shown as determined from the dispersion (2.11), and the corresponding $\mathrm{Re}(c\alpha/\Omega)$ for zero applied field and $1/\Omega\tau=0.0002$. The solid line is $|\mathrm{Im}(k_x)|$ and the dashed line is $\mathrm{Re}(\alpha)$. $\mathrm{Im}(k_x)$ becomes large only in the bulk band and near ω_s. In the surface mode region, $\mathrm{Im}(k_x)$ is small so the wave has a long path length. $\mathrm{Re}(\alpha)$ is very large for frequencies below ω_s and above the bulk band, thus indicating a strong localization to the surface. The localization is strongest near the bulk band limit, $\omega/\Omega=1$. In the bulk band, however, $\mathrm{Re}(\alpha)$ is small and so the mode in this region is weakly bound to the surface.

Damping allows the surface mode to lose energy into the material. In Fig. 5, the $+k_x$ branch of the dispersion curve plus the decay parameters $\mathrm{Im}(k_x)$ and $\mathrm{Re}(\alpha)$ are plotted for $1/\omega\tau=0.0008$. The solid line is $|\mathrm{Im}(k_x)|$ and the dashed line is $\mathrm{Re}(\alpha)$. H_0 is still zero. With greater damping the surface mode is not as tightly bound to the surface as before and penetrates further into the material. This increases the rate of energy loss into the material and thus the surface mode has a shorter path length. In this way damping allows the modes to "leak" energy into the interior of the material.

In an applied field, the surface modes outside the bulk bands are highly nonreciprocal. The resonances in the

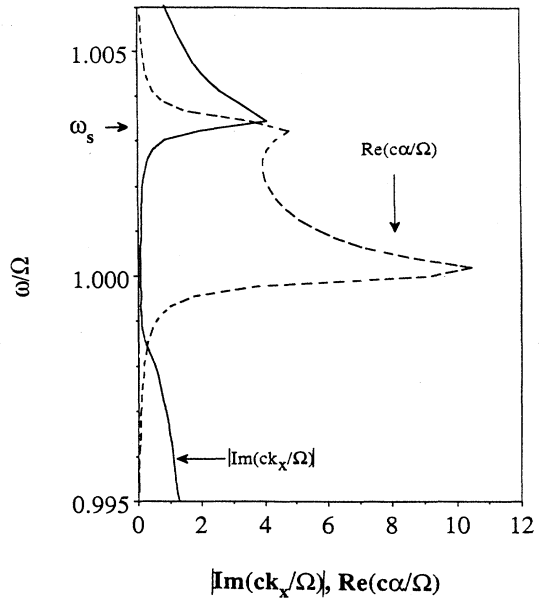

FIG. 4. Decay parameter $|\mathrm{Im}(ck_x/\Omega)|$ and localization parameter $\mathrm{Re}(c\alpha/\Omega)$ for the $+k_x$ branch of the $1/\Omega\tau=0.0002$ dispersion curve of Fig. 2. Only the magnitudes are shown. The solid line is $\mathrm{Im}(k_x)$ and the dashed line is $\mathrm{Re}(c\alpha/\Omega)$. Note the strong localization to the surface just above $\omega/\Omega=1$. The localization is greatest in the surface mode region near the lower bulk band frequency limit.

bulk bands are also nonreciprocal in applied field, although the nonreciprocity disappears at frequencies below the lower bulk band limit. This is seen in Fig. 6 where the real part of k_x is plotted against frequency for $H_0=0.3$ kG. The dashed lines are the $1/\Omega\tau=0$ modes and the solid lines are the dissipative waves for $1/\Omega\tau=0.0002$. The $1/\Omega\tau=0$ modes coincide with the $1/\Omega\tau=0.0002$ modes except near the magnetostatic limit frequency. Again there is a close correspondence between the $1/\Omega\tau=0$ modes and the modes with damping in the surface mode region between the bulk band and the magnetostatic limit.

With the applied field, there are two regions where the real parts of γ and α become very small and the leaky modes become ill-defined. One region is above $\omega/\Omega=1.0075$, near the upper limit of the middle bulk band. The leaky modes do not seem to exist for frequencies above 1.0075. The second region occurs for the $+k_x$ branch near $\omega/\Omega=0.998$. Here γ becomes very small and the Brewster mode is ill-defined for frequencies between 0.998 and the top of the lower bulk band.

In Fig. 7, frequency versus $|\mathrm{Im}(k_x)|$ and $\mathrm{Re}(\alpha)$ are again shown, this time for the case of an applied field of 0.3 kG and $1/\Omega\tau=0.0002$. The solid lines are $|\mathrm{Im}(k_x)|$ and the dashed lines are $\mathrm{Re}(\alpha)$. Values for the $-k_x$ branch are shown in the top plot and values for the $+k_x$ branch are shown in the lower plot. Although signs are now shown, $\mathrm{Im}(k_x)$ is negative for the $-k_x$ branch so

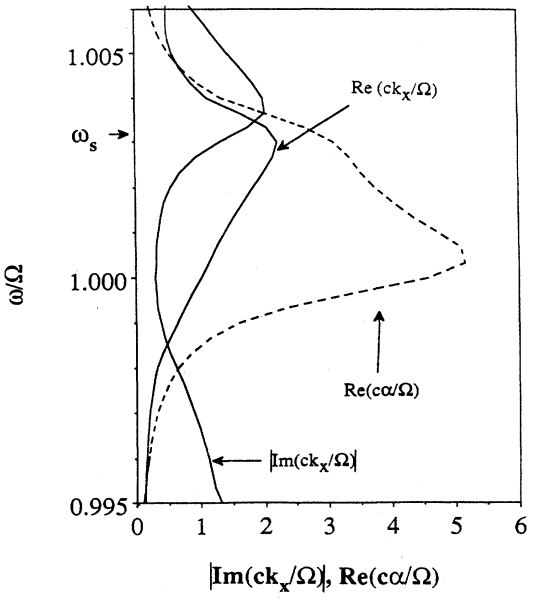

FIG. 5. Decay parameter $|\mathrm{Im}(ck_x/\Omega)|$ and localization parameter $\mathrm{Re}(c\alpha/\Omega)$ for the $+k_x$ branch of dispersion curves with $1/\Omega\tau=0.0008$. The solid line is $\mathrm{Im}(k_x)$ and the dashed line is $\mathrm{Re}(c\alpha/\Omega)$. There is no applied field and only the magnitudes are shown. Here the increased damping decreases the localization of the modes to the surface at all frequencies.

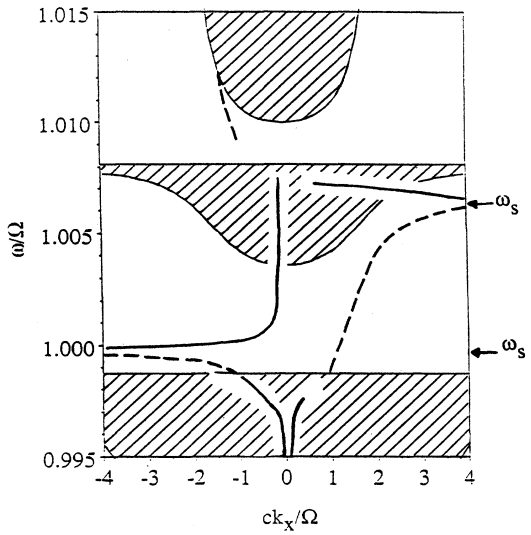

FIG. 6. Dispersion curves for antiferromagnetic polaritons, in MnF_2, with an applied field of 0.3 kG. The shaded areas are bulk bands and the dashed lines are the surface modes when there is no damping present in the material. The solid lines show how damping modifies the surface mode frequencies. These solid lines are the real parts of the complex solutions to the dispersion relation (3.1) with damping $1/\Omega\tau=0.0002$. Note that the modes with damping present are reciprocal at low frequencies in the lower bulk band and become highly nonreciprocal at higher frequencies.

that the wave attenuates in the $-x$ direction. Again there is strong localization to the surface in regions below ω_s and above the bulk band for both branches. Also note the strong localization of the surface modes where they begin near the light line (see Fig. 6) and the lack of localization as they enter the upper bulk band. Both branches are strongly bound to the surface near the lower bulk band limit and near ω_s. In between, however, the localization decreases. In both the $+k_x$ and $-k_x$ branches, the path length is large except in the lower bulk band and above ω_s. The path length is also large above the middle bulk band.

The power flows in surface excitations with damping present help clarify the nature of the leaky modes. Using the results of Camley and Mills,[7] it is a simple matter to calculate the amplitudes of the electric and magnetic fields of the surface polaritons inside and outside the material. From these one can calculate the Poynting's vector inside and outside the material. The total power flow parallel to the surface in the material is found by integrating the material Poynting's vector over a rectangular surface of width L_z from $y=0$ to $y=\infty$. Likewise, the total power flow parallel to the surface in the vacuum is found by integrating the vacuum Poynting's vector over a rectangular surface of width L_z from $y=0$ to $y=-\infty$.

Defining power flows per unit length as $U^{>}/L_z$ for the power flow in the material and $U^{<}/L_z$ for the power flow in the vacuum, one obtains the expressions

$$U^{<}=\frac{1}{2\mathrm{Re}(\beta)}\mathrm{Re}\left[\frac{c}{4\pi\omega_0}E_z^2 k_x\right] \tag{2.15}$$

and

$$U^{>}=\frac{1}{2\mathrm{Re}(\alpha)}\mathrm{Re}\left[\frac{c}{4\pi\omega_0}E_z^2\left[\frac{\mu_2\alpha^*-\mu_1 k_x}{\mu_1\alpha^*-\mu_2 k_x}\right]\beta^*\right]. \tag{2.16}$$

Here E_z is the amplitude of the electric field of the polaritons at the surface.

The parallel power flows $U^{>}$ and $U^{<}$ are plotted in Fig. 8 for the frequency and complex wave-vector solutions of (2.11) for $-k_x$ with no applied field and $1/\Omega\tau=0.0002$. In the bulk band ($\omega/\Omega<1$) the power flows inside and outside the material are both in the direction of propagation. At lower frequencies, most of the energy is carried by fields in the material. Near the bulk band limit, however, most of the energy is carried in the fields outside the material, and at the antiferromagnetic resonance frequency, $\omega/\Omega=1$, all of the electromagnetic energy is carried in the vacuum.

In the surface mode region above the bulk band and below ω_s, the energy in the material flows opposite to the direction of propagation. This is typical of surface plasmon and magnon polaritons. Note that in the surface

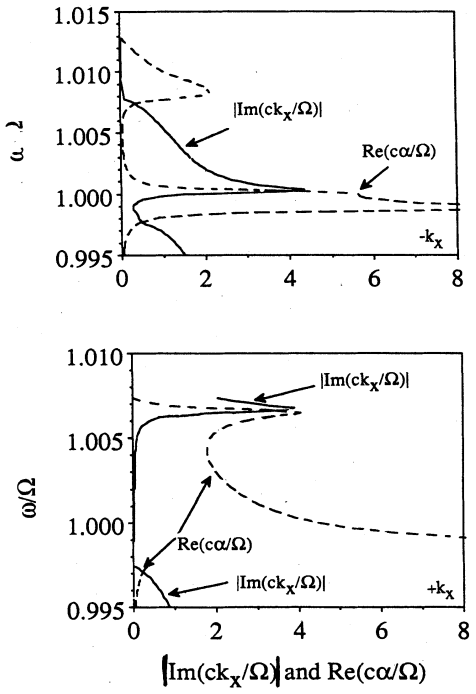

FIG. 7. Decay parameter $|\mathrm{Im}(ck_x/\Omega)|$ and localization parameter $\mathrm{Re}(c\alpha/\Omega)$ for the $+k_x$ and $-k_x$ branches of the $1/\Omega\tau=0.0002$ dispersion curves of Fig. 6. Again, only the magnitudes are shown. The solid lines are $\mathrm{Im}(k_x)$ and the dashed lines are $\mathrm{Re}(c\alpha/\Omega)$. The decay parameters for the $-k_x$ branch are shown in the upper plot and those of the $+k_x$ branch in the lower plot. Note again the strong localization to the surface just above the lowest bulk band limit.

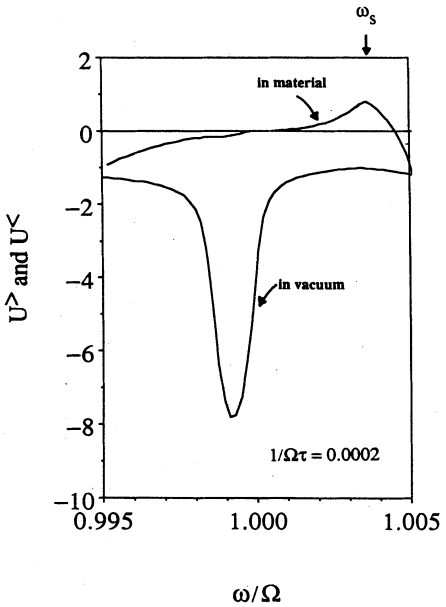

FIG. 8. Parallel power flows $U^{>}$ and $U^{<}$ for the $-k_x$ branch of $1/\Omega\tau=0.0002$ modes in zero applied field. Note that in the surface mode region between ω_s and the lower bulk band limit ($\omega/\Omega=1$) the energy flow inside the material is opposite the direction of propagation.

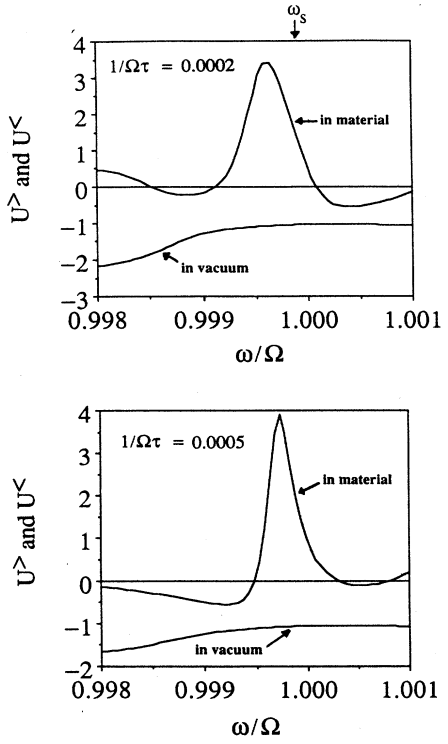

FIG. 9. Parallel power flows $U^>$ and $U^<$ for the $-k_x$ branches of $1/\Omega\tau=0.0002$ modes with a 0.3 kG applied field. The upper plot is for the case of $1/\Omega\tau=0.0002$ and the lower plot is for the case $1/\Omega\tau=0.0005$. Note that the direction of power flow inside the material is strongly influenced through the nonzero μ_2 term.

wave region, most of the energy is carried by the fields in vacuum and so the net energy flow is in the direction of propagation except near the magnetostatic frequency. At ω_s the electromagnetic energy carried by the fields in vacuum is nearly equal to the energy carried in the opposite direction by the fields in the material and the net energy flow is very small. Above ω_s, the energy flow is in the direction of propagation both in the material and outside.

The power flows $U^>$ and $U^<$ are plotted in Fig. 9 for the frequency and complex wave-vector solutions of (2.11) with an applied field $H_0=0.3$ kG. The damping is $1/\Omega\tau=0.0002$ in the upper plot and 0.0005 in the lower plot. Here only the $-k_x$ solutions are shown. For both dampings, energy flow in the material is opposite the direction of propagation for frequencies near ω_s. Near the bulk band, however, the energy flow in the material is in the direction of propagation. Furthermore, comparison of the upper and lower plots shows that increasing the damping decreases the frequency range for energy flow in the material that opposes the direction of propagation.

The direction of energy flow in the material is governed by the sign and magnitude of the magnetic susceptibilities. A negative μ_1 usually leads to energy flows opposite the direction of propagation. This occurs in the surface mode region when there is no applied field. Also with no applied field, μ_1 is positive in the bulk band and the energy flow is in the direction of propagation. In an applied field, however, the nonvanishing μ_2 can lead to positive energy flows in the surface region and negative energy flows in the bulk, near the bulk band limits. This is because near the limit frequencies $\Omega\pm\gamma H_0$, α, μ_1, and μ_2 are extremely sensitive to frequency. Consequently, near Ω the direction of the power flow is very sensitive to the introduction of an applied field. In addition, damping also plays an important role near the bulk band limits, as seen by comparing the two plots of Fig. 9.

III. GREEN'S FUNCTIONS

In this section the Green's functions appropriate to a semi-infinite antiferromagnet are calculated. To simplify the algebra, only Green's functions with the electric field parallel to the easy axis are calculated explicitly. Finally, the surface-polariton modes and leaky modes discussed in Sec. II are shown also to be represented by the Green's functions.

The driven magnetic wave equation for the propagation of electromagnetic waves in media described by the susceptibilities (2.3) and (2.8) has the form

$$\epsilon_k \sum_{j,m}{}' \left[\epsilon_m^{-1} \frac{\partial^2}{\partial x_j \partial x_k} - \delta_{jk} \left[\sum_l \epsilon_m^{-1} \frac{\partial^2}{\partial x_l^2} \right] - \omega_0^2 \mu_{kj} \right] H_j = F_k \ . \tag{3.1}$$

Here F is the driving field. Note that both the magnetic fields H and the driving fields F are assumed to have time dependance $e^{-i\omega t}$.

The Green's functions satisfy the associated wave equation given by

$$\epsilon_k \sum_{m,j}{}' \left[\epsilon_m^{-1} \frac{\partial^2}{\partial x_j \partial x_k} - \delta_{jk} \left[\sum_l \epsilon_m^{-1} \frac{\partial^2}{\partial x_l^2} \right] - \omega_0^2 \mu_{kj} \right] g_{jm}(\mathbf{x},\mathbf{x}') = 4\pi \delta_{km} \delta(\mathbf{x}-\mathbf{x}') \ . \tag{3.2}$$

The solutions to (3.1) are then given by

$$H_j = \sum_k \int d\mathbf{x}' g_{jk}(\mathbf{x},\mathbf{x}') F_k \ . \tag{3.3}$$

The volume of integration is over all of space.

Equation (3.2) must be translationally invariant in both x and z. This invariance can be exploited through the use of Fourier expansions:

$$g_{jk}(\mathbf{x},\mathbf{x}')=\int_{-\infty}^{\infty}\frac{d^2\mathbf{k}_\parallel}{4\pi^2}e^{i\mathbf{k}_\parallel\cdot(\mathbf{x}_\parallel-\mathbf{x}'_\parallel)}g_{jk}(\mathbf{k}_\parallel;y,y') \ . \tag{3.4}$$

and

$$\delta(\mathbf{x}-\mathbf{x}')=\delta(y-y')\int_{-\infty}^{\infty}\frac{d^2\mathbf{k}_\parallel}{4\pi^2}e^{i\mathbf{k}_\parallel\cdot(\mathbf{x}_\parallel-\mathbf{x}'_\parallel)} \ . \tag{3.5}$$

Here we have made the definitions $\mathbf{k}_\parallel=\hat{\mathbf{x}}k_x+\hat{\mathbf{z}}k_z$ for the wave vector parallel to the plane $t=0$ and $\mathbf{x}_\parallel=\hat{\mathbf{x}}x+\hat{\mathbf{z}}z$ for the position vector in that plane.

Applying these transformations to the Green's function equation (3.2), and writing the result in explicit matrix form,

$$\begin{bmatrix} \frac{\epsilon_1}{\epsilon_2}D^2-k_1^2 & i\left[\omega_0^2\mu_2\epsilon_1-\frac{\epsilon_1}{\epsilon_2}k_xD\right] & k_xk_z \\ -i\left[\omega_0^2\epsilon_1\mu_2+\frac{\epsilon_1}{\epsilon_2}k_xD\right] & -\left[\frac{\epsilon_1}{\epsilon_2}k_x^2+k_1^2\right] & -ik_zD \\ k_xk_z & -ik_zD & D^2-k_2^2 \end{bmatrix}\overleftrightarrow{g}=-4\pi\overleftrightarrow{I}\delta(y-y') \ , \tag{3.6}$$

with the definitions

$$D=\partial/\partial_y \ , \tag{3.7}$$

$$k_1^2=k_z^2-\omega_0^2\epsilon_1\mu_1 \ , \tag{3.8}$$

$$k_2^2=k_x^2-\omega_0^2\epsilon_2 \ . \tag{3.9}$$

The electric and magnetic fields must satisfy the usual homogeneous electromagnetic boundary conditions at the surface $y=0$ (assuming that the sources of the driving fields are not located at the surface $y=0$ so that the boundary conditions are homogeneous). The condition that the normal component of **B** be continuous across $y=0$ is first applied. Using the **H** field given by Eq. (3.3) to calculate **B**, applying the boundary condition and equating coefficients of F_k results in the condition

$$[-i\mu_2g_{xm}+\mu_1g_{ym}]_{y=0+}=[g_{ym}]_{y=0-} \ . \tag{3.10}$$

Similarly, continuity of tangential **H** results in

$$[g_{xm}]_{y=0+}=[g_{xm}]_{y=0-} \ , \tag{3.11}$$

$$[g_{zm}]_{y=0+}=[g_{zm}]_{y=0-} \ . \tag{3.12}$$

Finally, relating **E** to **H** via Maxwell's relations, continuity of tangential **E** requires that

$$[iDg_{zm}+k_zg_{ym}]_{y=0+}=\epsilon_2[iDg_{zm}+k_zg_{ym}]_{y=0-} \ , \tag{3.13}$$

$$[k_xg_{ym}+iDg_{xm}]_{y=0+}=\epsilon_2[k_xg_{ym}+iDg_{xm}]_{y=0-} \ . \tag{3.14}$$

Combining Eqs. (3.11) and (3.12) gives an equation identical to that which arises by requiring continuity of normal **D** across $y=0$, and thus provides no new information.

The complexity of the algebra makes an analytical solution for the case of general propagation directions difficult. The main features of interest, however, can be had by considering the simpler case where the electric field is constrained to lie along the z axis and the incident electromagnetic wave propagates in the xy plane. This is called the Voigt geometry and is a common experimental set up. In addition, the nonreciprocity is often a maximum in this geometry. The Voigt geometry uncouples the H_z field from the H_x and H_y fields, as can be seen by examining the equation of motion matrix (3.6). This greatly facilitates the separation and solution of the differential equations of motion and the application of the boundary conditions.

Note that in the special case of the electric field along $\hat{\mathbf{z}}$, $\overleftrightarrow{g}$ has no z dependence and thus its Fourier expansion is in one dimension only. Accordingly, the wave equation (3.2) is transformed with the one-dimensional counterparts of the transforms (3.4) and (3.5).

Green's functions for sources outside of the material

The Green's functions differ depending on whether the source point y' lies in the material or outside in vacuum. Beginning with the case where y' lies outside the material, the matrix equation for $\overleftrightarrow{g}$ becomes

$$\begin{bmatrix} D^2+\omega_0^2\epsilon_2\mu_1 & i(\omega_0^2\epsilon_2\mu_2-k_xD) \\ -i(\omega_0^2\epsilon_2\mu_2+k_xD) & -i(k_x^2-\omega_0^2\epsilon_2\mu_1) \end{bmatrix}\overleftrightarrow{g}(k_y;y,y')=0 \tag{3.15}$$

for $y>0$ and $y'<0$ (source outside the material and observation point inside the material). In this polarization there is no z component of the H field so $\overleftrightarrow{g}$ is now a 2×2 matrix. The homogeneous set of Eqs. (3.15) have the solutions

$$g_{ij}^h=C_{ij}^{>}e^{-\alpha y} \ , \tag{3.16}$$

where α represents the decay constant in the y direction and is given by (2.12). Note that the positive root is specified to insure proper decay in the y direction. The coefficients $C_{ij}^{>}$ in (3.16) will be determined later through the boundary conditions.

For fields outside the material, the appropriate Green's functions satisfy the inhomogeneous equations

$$\begin{bmatrix} D^2+\omega_0^2 & -ik_xD \\ -ik_xD & \omega_0^2-k_x^2 \end{bmatrix} \overleftrightarrow{g}(k_x;y,y') = -4\pi \overleftrightarrow{I}\delta(y-y') \quad (3.17)$$

for $y<0$ and $y'<0$.

The solutions to this set of equations will be a linear combination of a particular solution, which solves the inhomogeneous equation, and a solution to the associated homogeneous equation. Thus,

$$g_{ij}=g_{ij}^h+g_{ij}^p \ , \quad (3.18)$$

where g_{ij}^h is the homogeneous solution and g_{ij}^p is the particular solution.

The particular solutions obey

$$(D^2-\beta^2)g_{xx}^p = -\frac{4\pi\beta^2}{\omega_0^2}\delta(y-y') \quad (3.19)$$

and

$$(D^2-\beta^2)g_{xy}^p = -\frac{4\pi ik_x}{\omega_0^2}D\delta(y-y') \ . \quad (3.20)$$

Here β is the decay constant in the y direction outside the material given by (2.13).

The solutions to Eqs. (3.19) and (3.20) must either vanish at $\pm\infty$ or must represent outgoing waves in order to be physical solutions. The solutions which vanish at ∞ are given by

$$(D^2-a^2)\frac{-e^{-a|y-y'|}}{2a} = \delta(y-y') \quad (3.21)$$

and

$$(D^2-a^2)\tfrac{1}{2}\mathrm{sgn}(y-y')e^{-a|y-y'|} = D\delta(y-y') \ , \quad (3.22)$$

with the condition that $\mathrm{Re}(a)$ is positive.

Our Green's functions will thus contain terms of the form $\exp(-\beta|y-y'|)$ and $\exp(-\alpha|y-y'|)$. If one is working in a region of the (ω,k_x) space where γ and α are purely real, there are no problems in choosing the correct sign for β and α.

In contrast, if β and α are purely imaginary, then one must choose the signs of β and α so that the Green's functions represent outgoing waves. With the forms above, one normally would expect the conditions

$$\mathrm{Im}(\beta)<0 \ , \quad (3.23)$$

$$\mathrm{Im}(\alpha)<0 \quad (3.24)$$

to be correct. However, it is not immediately obvious that this is the correct choice since it is the group velocity, and not the phase velocity, which has physical meaning. An explicit example of such considerations can be found in Ref. 16.

Finally, we consider the case where α and β are complex. Such a situation occurs, for example, when damping is present in both media. In principle, one might want to specify both exponential decay *and* outgoing waves for physical sense. However, one cannot generally choose the sign on both the real and imaginary parts of α and β independently. The sign of τ determines whether the imaginary and real parts of α have the same sign or not, for example. We will see that in order to get the maximum information from the Green's functions we will have to slightly relax our boundary conditions.

The particular solutions to Eqs. (3.19) and (3.20) are

$$g_{xx}^p = \frac{2\pi\beta}{\omega_0^2}e^{-\beta|y-y'|} \ , \quad (3.25)$$

$$g_{xy}^p = -\frac{2\pi ik_x}{\omega_0^2}\mathrm{sgn}(y-y')e^{-\beta|y-y'|} \ . \quad (3.26)$$

The homogeneous solutions to the equation set (3.17) are given by

$$g_{ij}^h = C_{ij}^{\lessgtr}e^{\beta y} \ . \quad (3.27)$$

The next task is to derive and apply boundary conditions to determine the coefficients C_{ij}. First, the homogeneous equations of motion (3.15) are examined. These provide a relationship between g_{xx} and g_{yx} valid as y approaches 0 from the positive side:

$$[i(\omega_0^2\epsilon_2\mu_2+k_xD)g_{xx}+(k_x^2-\omega_0^2\epsilon_2\mu_1)g_{yx}]_{y=0+}=0 \ . \quad (3.28)$$

Similarly, the equations of motions in (3.17) provide a relationship valid when y approaches 0 from the negative:

$$[ik_xDg_{xx}+(k_x^2-\omega_0^2)g_{yx}]_{y=0-}=0 \ . \quad (3.29)$$

Together with the continuity condition on normal **B** from Eq. (3.10), these relations result in a boundary condition on g_{xx}:

$$[(\omega_0^2\epsilon_2\mu_1-k_x^2)Dg_{xx}]_{y=0-}=[-\beta^2(\mu_2k_x+\mu_1D)g_{xx}]_{y=0+} \ . \quad (3.30)$$

The continuity condition of tangential **H** given in (3.11) provides a second boundary condition on g_{xx}.

For $y>0$, the solution g_{xx} is given by Eq. (3.16). For $y<0$, g_{xx} also includes the particular solution (3.25) in addition to the homogeneous part (3.27). Application of the boundary conditions (3.11) and (3.30) determine the coefficients C_{xx} from the homogeneous parts of the solutions and result in the following expressions for the solutions in each region. For $y'<0$ and $y>0$,

$$g_{xx}^+ = \frac{4\pi\beta}{\omega_0^2}\left[\frac{A}{A-B}\right]e^{\beta y'}e^{-\alpha y} \ , \quad (3.31)$$

and for $y'<0$ and $y<0$,

$$g_{xx}^- = \frac{2\pi\beta}{\omega_0^2}\left[\frac{A\ \mathrm{sgn}(y-y')+B}{A-B}e^{-\beta(y+y')}+e^{-\beta|y-y'|}\right] . \quad (3.32)$$

The quantities A and B are defined as

$$A=\omega_0^2\epsilon_2\mu_1-k_x^2 \ , \quad (3.33)$$

$$B=\beta(\mu_1\alpha-\mu_2k_x) \ . \quad (3.34)$$

The poles of the Green's functions occur when $A-B=0$. This condition can be shown to give the antiferromagnetic surface polariton dispersion relation derived by Camley and Mills.[7]

The relationships between g_{xx} and g_{yx} given in the equations of motion (3.15) and (3.17) can be used to easily determine g_{yx} from Eqs. (3.31) and (3.32). The result for $y'<0$ and $y>0$ is

$$g_{yx}^{+}=\frac{4\pi i\beta}{\omega_0^2}\left[\frac{\omega_0^2\epsilon_2\mu_2-\alpha k_x}{A-B}\right]e^{\beta y'}e^{-\alpha y}\ , \tag{3.35}$$

while for $y'<0$ and $y<0$,

$$g_{yx}^{-}=-\frac{2\pi i k_x}{\omega_0^2}\left[\frac{A\ \mathrm{sgn}(y-y')+B}{A-B}e^{\beta(y+y')}-\mathrm{sgn}(y-y')e^{-\beta|y-y'|}\right]\ . \tag{3.36}$$

The remaining Green's functions are found in much the same manner. The particular solution for g_{xy} is given by (3.26), but boundary conditions are still required to find $C_{xy}^{>}$ and $C_{xy}^{<}$ for the homogeneous solutions given by (3.16) and (3.27). Note that in this problem the source terms do not lie at $y'=0$, so only the homogeneous counterparts of the inhomogeneous equations belonging to (3.17) are used to uncouple the boundary conditions for g_{xy}. In particular, from (3.17) a relationship valid at $y=0-$ is obtained:

$$[\beta^2 g_{yy}+ik_x Dg_{xy}]_{y=0-}=0\ . \tag{3.37}$$

The corresponding relation in (3.15) is:

$$[i(\omega_0^2\epsilon_2\mu_2+k_x D)g_{xy}+(\omega_0^2\epsilon_2\mu_1-k_x^2)g_{yy}]_{y=0+}=0\ . \tag{3.38}$$

As before, this is combined with the continuity equation on normal **B** (3.10) to derive the boundary condition

$$[-\beta^2(\mu_2 k_x+\mu_1 D)g_{xy}]_{y=0+}=[(\omega_0^2\epsilon_2\mu_1-k_x^2)Dg_{xy}]_{y=0-}\ . \tag{3.39}$$

Again, the continuity of tangential **H** (3.11) provides a second boundary condition.

Application of these conditions on the solutions given by (3.16) for $y>0$ and the sum of (3.26) and (3.27) for $y>0$ determine C_{xy}. The resulting expression for g_{xy} for $y'<0$ and $y>0$ is

$$g_{xy}^{+}=-\frac{4\pi i k_x}{\omega_0^2}\left[\frac{A}{A-B}\right]e^{\beta y'}e^{-\alpha y}\ , \tag{3.40}$$

and the expression

$$g_{xy}^{-}=\frac{2\pi i k_x}{\omega_0^2}\left[\frac{A+\mathrm{sgn}(y-y')B}{A-B}e^{\beta(y+y')}-\mathrm{sgn}(y-y')e^{-\beta|y-y'|}\right] \tag{3.41}$$

is for $y'<0$ and $y<0$.

Finally, the equations of motion in (3.15) and (3.17) are used to determine g_{yy} from the g_{xy} of Eqs. (3.40) and (3.41). The result for $y'<0$ and $y>0$ is

$$g_{yy}^{+}=\frac{4\pi k_x}{\omega_0^2}\left[\frac{\omega_0^2\epsilon_2\mu_2-\alpha k_x}{A-B}\right]e^{\beta y'}e^{-\alpha y}\ . \tag{3.42}$$

For $y'<0$ and $y<0$ the inhomogeneous term from (3.17) must be included:

$$g_{yy}^{-}=\frac{2\pi k_x^2}{\omega_0^2\beta}\left[\frac{A+\mathrm{sgn}(y-y')B}{A-B}e^{\beta(y+y')}+e^{-\beta|y-y'|}\right]+\frac{4\pi}{\beta^2}\delta(y-y')\ . \tag{3.43}$$

The above Green's functions reduce to those of Mills and Maradudin[10] in the nonmagnetic limit $\mu_1=1$, $\mu_2=0$, and $\epsilon_1=\epsilon_2$.

Green's functions for sources inside the material

When the source points are in the material ($y'>0$), the Green's functions satisfy inhomogeneous equations for $y>0$ (in the material) given by

$$\begin{bmatrix} D^2+\omega_0^2\epsilon_2\mu_1 & i(\omega_0^2\epsilon_2\mu_2-k_x D) \\ -i(\omega_0^2\epsilon_2\mu_2+k_x D) & -(k_x^2-\omega_0^2\epsilon_2\mu_1)\end{bmatrix}\overleftrightarrow{g}(k_y;y,y')=-\frac{4\pi\epsilon_2}{c\epsilon_1}\overleftrightarrow{I}\delta(y-y') \tag{3.44}$$

and homogeneous equations for $y<0$ (outside the material) given by

$$\begin{bmatrix} D^2+\omega_0^2 & -ik_x D \\ -ik_x D & \omega_0^2-k_x^2\end{bmatrix}\overleftrightarrow{g}(k_x;y,y')=0\ . \tag{3.45}$$

These equations can be uncoupled and solved for the homogeneous and particular solutions g_{ij}, just as in the case where $y'<0$. Also, one can derive boundary conditions in the same manner as before that are identical to those of Eqs. (3.30) and (3.31). With the definition

$$C=-\beta[\mu_1\alpha\,\mathrm{sgn}(y-y')+\mu_2 k_x]\ , \tag{3.46}$$

this prescription results in the following Green's functions for $y>0$ and $y>0$:

$$g_{xx}^{+}=\frac{2\pi A}{\alpha\omega_0^2\epsilon_1\mu_1}\left[\left[\frac{A-C}{A-B}\right]e^{-\alpha(y+y')}-e^{-\alpha|y-y'|}\right]\ , \tag{3.47}$$

$$g_{xy}^{+}=-\frac{2\pi A}{\alpha\omega_0^2\epsilon_1\mu_1}\left[\left[\frac{A-C}{A-B}\right]e^{-\alpha(y+y')}-e^{-\alpha|y-y'|}\right][\omega_0^2\mu_2\epsilon_2-\alpha k_x\,\mathrm{sgn}(y-y')]\ , \tag{3.48}$$

$$g_{yy}^{+}=\frac{2\pi i[\omega_0^2\mu_2\epsilon_2-\alpha k_x\,\mathrm{sgn}(y-y')]}{\alpha\omega_0^2\epsilon_1\mu_1 A}\left\{\omega_0^2\epsilon_2\mu_2\left[e^{-\alpha|y-y'|}-\left[\frac{A-C}{A-B}\right]e^{-\alpha(y+y')}\right]\right.$$
$$\left.-\alpha k_x\left[\mathrm{sgn}(y-y')e^{-\alpha|y-y'|}-\left[\frac{A-C}{A-B}\right]e^{-\alpha(y+y')}\right]\right\}+\frac{4\pi\epsilon_2}{\epsilon_1 A}\delta(y-y')\,, \quad (3.49)$$

$$g_{yx}^{+}=\frac{2\pi i}{\alpha\omega_0^2\epsilon_1\mu_1}\left\{\omega_0^2\epsilon_2\mu_2\left[\left[\frac{A-C}{A-B}\right]e^{-\alpha(y+y')}-e^{-\alpha|y-y'|}\right]+\alpha k_x\left[\mathrm{sgn}(y-y')e^{-\alpha|y-y'|}-\left[\frac{A-C}{A-B}\right]e^{-\alpha(y+y')}\right]\right\}. \quad (3.50)$$

For $y<0$ and $y'>0$,

$$g_{xx}^{-}=\frac{4\pi AB}{\alpha\omega_0^2\epsilon_1\mu_1}\left[\frac{1}{A-B}\right]e^{\beta y}e^{-\alpha y'}\,, \quad (3.51)$$

$$g_{xy}=\frac{-4\pi iB}{\alpha\omega_0^2\epsilon_1\mu_1}\left[\frac{1}{A-B}\right](\omega_0^2\epsilon_2\mu_2+\alpha k_x)e^{\beta y}e^{-\alpha y'}\,, \quad (3.52)$$

$$g_{yy}^{-}=\frac{-4\pi Bk_x}{\beta\alpha\omega_0^2\epsilon_1\mu_1}\left[\frac{1}{A-B}\right](\omega_0^2\epsilon_2\mu_2+\alpha k_x)e^{\beta y}e^{-\alpha y'}\,, \quad (3.53)$$

$$g_{yx}=\frac{-4\pi iABk_x}{\alpha\beta\omega_0^2\epsilon_1\mu_1}\left[\frac{1}{A-B}\right]e^{\beta y}e^{-\alpha y'}\,. \quad (3.54)$$

Surface-polariton and leaky mode excitations

When the g_{ij} are considered as functions of k_x for an ω fixed in the surface-polariton region, the g_{ij} have sharp peaks at those k_x that satisfy the surface-polariton relation. To illustrate this, in Fig. 10 g_{xx} (evaluated at the surface just inside the material) is plotted versus the unitless wave vector ck_x/Ω for $\omega/\Omega=1.002$ and $\omega/\Omega=0.9989$. For simplicity, there is no applied field and a damping of $1/\Omega\tau=0.0002$ so that the peaks have finite width.

The 1.002 peak occurs at a k_x where a surface polariton exists. In this plot, the signs of α and γ were chosen for exponential decay inside and outside the material. By using an appropriate branch cut definition, this sign convention can be represented symbolically through a complex frequency as the limit of $g_{xx}(\omega+i\eta)$ as η goes to zero from the positive side. The spectral density is proportional to $-i\,\mathrm{Im}[g_{ij}(\omega+i\eta)]$, so the negative peak in $\mathrm{Im}[g_{xx}(\omega+i\eta)]$ insures a positive spectral density.[1]

In contrast, the curve for $\omega/\Omega=0.9989$ cannot be understood as representing a spectral density. It represents a different excitation in a frequency region forbidden to surface polaritons. This excitation is unlike the "true" surface polaritons in that it has a significantly large radiative part in directions normal to the surface. Also, $\mathrm{Im}(g_{xx})$ is zero at the wave vector of the excitation and has opposite signs on either side of the excitation's wave vector. The peak, as shown in Fig. 10, occurs instead in the real part of g_{xx}.

As discussed in the derivation of the Green's functions, care must be taken in choosing the appropriate signs on the real parts of γ and α in order to satisfy the exponential decay boundary condition at $y=\pm\infty$. When these conditions are strictly obeyed, the surface-polariton peak at $\omega/\Omega=1.002$ exists but the peak at $\omega/\Omega=0.9989$ does not. The peak at $\omega/\Omega=0.9989$ was produced by choosing the sign of α to represent a wave with a large radiative part but with a small exponential increase as y goes to $+\infty$. The rate of increase depends on the damping. The sign on γ was still chosen for exponential decay for $y<0$.

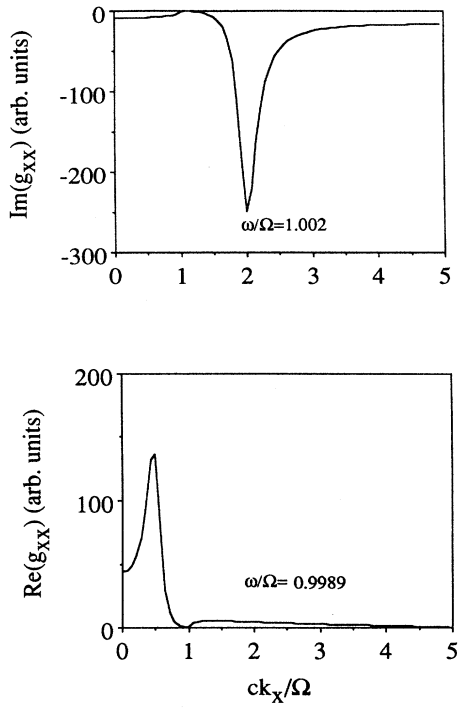

FIG. 10. Poles of g_{xx} at $\omega/\Omega=1.002$ and $\omega/\Omega=0.9989$ as functions of ck_x/Ω. There is no applied field and $1/\omega\tau=0.0002$. The $\omega/\Omega=1.002$ peak occurs at the $+k_x$ surface polariton of Fig. 2. Note the existence of an excitation in the $\omega/\Omega=0.9989$ curve that lies in a frequency region forbidden to surface polaritons.

The dependence on "nonphysical" boundary conditions at ∞ is a characteristic of the leaky modes and has received a great deal of attention in the literature.[17–19] Leaky modes are not eigenmodes of the system, and their existence is strongly dependent on the geometry of the sample and the driving electromagnetic fields. Leaky modes are typically represented as exponentially increasing into the material, with the understanding that absorption by the material prevents unbounded growth. The use of these Green's functions to show their existence is only an approximation and is justified mainly by the fact that leaky modes are observed in experiment and account for significant losses from the radiation fields.[19]

An approximation that relaxes the boundary conditions at ∞ allows the Green's functions with damping to show excitations at real frequencies and real wave vectors that represent magnetic Brewster modes. A dispersion relation can be obtained from the Green's functions in the following way. Fix a value of ω and plot $g(k,\omega)$ as a function of k_x. The value of k_x for which there is a peak and the initial value of ω provide one point of a dispersion curve. By repeating the process for different ω values, one can trace out the entire dispersion curve.

Figure 11 presents the comparison between the Green's function results and the results from Eq. (2.11) with zero applied field. Here $1/\Omega\tau=0.0001$, and only the region near the resonance inside the bulk band is examined. The two curves represent the results from (2.11) for ω versus $\mathrm{Re}(k_x)$ and the Green's function results for ω versus k_x. The Green's function and the $\mathrm{Re}(k_x)$ curves are in reasonable agreement at smaller frequencies and they approach one another as the frequency increases. The behavior of the imaginary part of the k_x as a function of frequency explains this. $\mathrm{Im}(k_x)$ is large at the lower frequencies, while at higher frequencies $\mathrm{Im}(k_x)$ is much smaller. Since the peaks in the Green's function occur at real wave vectors, good agreement with the dispersion relation results when k_x is not expected to have a large imaginary part.

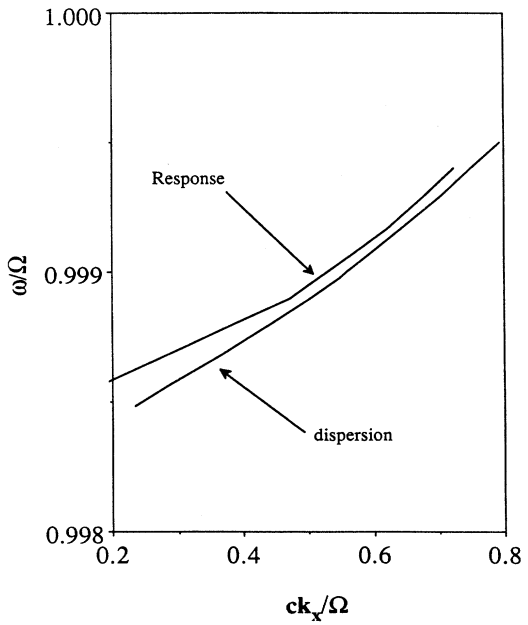

FIG. 11. The surface resonance poles of g_{xx} as functions of real ω and real k_x with damping $1/\omega\tau=0.0001$. There is no applied field. Also plotted is the dispersion curve of the surface resonance obtained by solving the damped dispersion relation (2.11) with real frequency and complex k_x. The g_{xx} poles approach the dispersion curve at higher frequencies where $\mathrm{Im}(ck_x/\Omega)$ becomes small.

We emphasize that even without the boundary condition approximation for leaky waves, the Green's functions and the dispersion curves obtained by solving (2.11) are fundamentally different things. Equation (2.11) describes possible excitations that may exist on the material, and the Green's functions describe the propagation of waves, originating from some source, through the material. In the dispersion description, the wave attenuates according to the imaginary part of the wave-vector solution. The response function, in contrast, has peaks at real frequencies and wave-vectors, and it is the width of the peaks that can be related to the attenuation of the wave. In paper II, we will use the Green's functions calculated here to discuss the scattering of electromagnetic waves from an antiferromagnet with rough surfaces.

IV. SUMMARY

A study of the antiferromagnetic surface-polariton dispersion curves revealed that with damping present in the material, there exist surface resonances in frequency regions forbidden to "true" antiferromagnetic surface polaritons. These surface resonances are the magnetic analog of the Brewster and evanescent modes found in plasmon-polariton studies. They have finite path lengths and can be highly dissipative with large penetration depths into the material. Like the surface-polariton modes, the surface waves with damping present are reciprocal when there is no applied field. In an applied field, they are nearly reciprocal at low frequencies within the lowest bulk band and become nonreciprocal at higher frequencies. The direction of the energy flow of leaky modes inside the material is extremely sensitive to damping and applied fields near the antiferromagnetic resonance frequencies.

The Green's functions for a semi-infinite antiferromagnet were calculated and used to approximate the material's response to a leaky mode. In the Green's function representation, the leaky modes are found to have characteristics consistent with previous studies: Largely radiative in character, the leaky modes have an amplitude that increases slowly with distance away from the surface into the material, representing energy "leaking" away from the surface into the bulk.

ACKNOWLEDGMENTS

The work of R.L.S. was supported by the Air Force Office of Scientific Research, Bolling Air Force Base, Washington D.C. The work of R.E.C. was supported by the Army Research Office under Contract No. DAAL03-88-88-K-0061.

[1]See the book, *Electromagnetic Surface Modes,* edited by A. D. Boardman (Wiley, New York, 1982).
[2]G. N. Zhihin, M. A. Moskalova, A. A. Sigarev, and V. A. Yakovelev, Opt. Commun. **43**, 32 (1982).
[3]See the review article by E. F. Sarmento and D. R. Tilley in Ref. 1.
[4]A. Hartstein, E. Burstein, A. A. Maradudin, R. Brewer, and R. F. Wallis, J. Phys. C **6**, 1266 (1973).
[5]L. Remer, B. Lüthi, H. Sauer, R. Beick, and R. E. Camley, Phys. Rev. Lett. **56**, 2752 (1986). There is some earlier work on bulk polaritons in antiferromagnets—see, for example, R. W. Sanders, R. M. Belanger, M. Motokawa, and V. Jaccarino, Phys. Rev. B **23**, 1190 (1981).
[6]A review of nonreciprocal surface waves is given by R. E. Camley, Surf. Sci. Rep. **7**, 103 (1987).
[7]R. E. Camley and D. L. Mills, Phys. Rev. B **26**, 1280 (1982); C. Shu and A. Caillé, Solid State Commun. **42**, 233 (1982).
[8]M. G. Cottam and A. A. Maradudin, in *Surface Excitations,* edited by V. M. Agranovich and R. Louden (Elsevier Science, New York, 1984), p. 1-194.
[9]D. L. Mills, Phys. Rev. B **12**, 4036 (1975).
[10]A. A. Maradudin and D. L. Mills, Phys. Rev. B **11**, 1892 (1975).
[11]A. A. Maradudin and W. Zierau, Phys. Rev. B **14**, 484 (1976).
[12]A. A. Maradudin and R. F. Wallis, J. Raman Spectrosc. **10**, 85 (1981).
[13]P. Halevi, in *Electric Surface Modes,* edited by A. D. Boardman (Wiley, New York, 1982), p. 249.
[14]D. L. Mills and E. Burstein, Rep. Prog. Phys. **37**, 817 (1974).
[15]R. E. Camley, Phys. Rev. Lett. **45**, 283 (1980).
[16]N. Raj, R. E. Camley, and D. R. Tilley, J. Phys. C **20**, 5208 (1987).
[17]G. I. Stegeman, J. J. Burke, and D. G. Hall, Opt. Lett. **8**, 383 (1983).
[18]C. W. Hsue and T. Tamir, J. Opt. Soc. Am. **A1**, 923 (1984).
[19]T. Tamir and A. A. Oliner, Proc. Inst. Electr. Eng. **110**, 310 (1963).